Monthly Notices of the ROYAL ASTRONOMICAL SOCIETY

MNRAS **466,** 546–555 (2017) doi:10.1093/mnras/stw3141
Advance Access publication 2016 December 5

Gaia's view of the λ Boo star puzzle

Simon J. Murphy[1,2★] and Ernst Paunzen[3]

[1]*School of Physics, Sydney Institute for Astronomy (SIfA), The University of Sydney, NSW 2006, Australia*
[2]*Department of Physics and Astronomy, Stellar Astrophysics Centre, Aarhus University, DK-8000 Aarhus C, Denmark*
[3]*Department of Theoretical Physics and Astrophysics, Masaryk University, Kotlářská 2, CZ-611 37 Brno, Czech Republic*

Accepted 2016 November 30. Received 2016 November 24; in original form 2016 October 19

ABSTRACT

The evolutionary status of the chemically peculiar class of λ Boo stars has been intensely debated. It is now agreed that the λ Boo phenomenon affects A stars of all ages, from star formation to the terminal age main sequence, but the cause of the chemical peculiarity is still a puzzle. We revisit the debate of their ages and temperatures in order to shed light on the phenomenon, using the new parallaxes in *Gaia* Data Release 1 with existing *Hipparcos* parallaxes and multicolour photometry. We find that no single formation mechanism is able to explain all the observations, and suggest that there are multiple channels producing λ Boo spectra. The relative importance of these channels varies with age, temperature and environment.

Key words: accretion, accretion discs – asteroseismology – stars: chemically peculiar – circumstellar matter – stars: distances – ISM: clouds.

1 INTRODUCTION

Chemically peculiar stars enable the study of astrophysical processes from a different perspective. At spectral type A, there are many classes of chemically peculiar stars, of which the Am and magnetic Ap stars are most common. Their slow rotation facilitates investigation of diffusion and mixing processes modulo the presence of a magnetic field. The λ Boo stars, which make up about 2 per cent of the population (Gray & Corbally 1998; Paunzen 2001), are the third most populous class. Unlike the Am and Ap stars, the λ Boo stars are moderate rotators (Abt & Morrell 1995) and the origin of their peculiarity remains a puzzle.

The abundance profile of λ Boo stars is characterized by depletions of Fe-peak elements of up to 2 dex (Andrievsky et al. 2002), but near-solar abundances of the volatile elements C, N, O and S (Baschek & Slettebak 1988; Kamp et al. 2001). This can be explained by the accretion of metal-poor material (Venn & Lambert 1990; Turcotte & Charbonneau 1993). In the circumstellar environment, the refractory elements that are incorporated into dust grains are prevented from accreting on to the A star by its strong radiation field, while the gas remains to be accreted freely (Waters, Trams & Waelkens 1992). However, the source of the accreting material is still uncertain. Suggestions have included accretion of material left-over from star formation (Holweger & Sturenburg 1993), stars passing through overdense regions of the interstellar medium (ISM; Kamp & Paunzen 2002) and the accretion of material ablated from hot Jupiters (Jura 2015). The gravitational influence of a jovian companion may further inhibit the migration of dust from a protoplanetary disc to the surface of the star (Kama, Folsom & Pinilla 2015).

Plenty of evidence suggests that λ Boo stars are young. They have been found in OB associations (Gray & Corbally 1993), they are absent from intermediate-age open clusters despite extensive searches (Gray & Corbally 2002), λ Boo abundance patterns are seen in several pre-main-sequence stars (Folsom et al. 2012) and luminosities from *Hipparcos* parallaxes place some λ Boo stars very close to the zero-age main sequence (ZAMS; Paunzen 1997). However, arguments to the contrary can also be found. Iliev & Barzova (1995) found they occupy a range of ages between 10^7 and 10^9 yr, and Iliev et al. (2002) found a binary pair of λ Boo stars with an age of 10^9 yr, ruling out a pre-main sequence status. A continuous source of accreting material must therefore be present, supplying 10^{-12}–10^{-11} $M_\odot$ yr^{-1} of material (Turcotte 2002), else the peculiarities are erased within 10^6 yr (Turcotte & Charbonneau 1993).

Attempts have been made to explain the λ Boo class as a heterogeneous group of stars that are not intrinsically chemically peculiar, but have composite spectra due to binarity instead (Faraggiana & Bonifacio 1999). Within the 'composite-spectrum hypothesis', the metal lines of one star are veiled by the continuum of the other and vice-versa, such that all metal lines *appear* peculiarly weak, but are not. The hypothesis was advocated in a series of papers by the same authors (e.g. Faraggiana, Gerbaldi & Bonifacio 2001), but was refuted in critical independent analyses (Stütz & Paunzen 2006; Griffin, Gray & Corbally 2012).

A significant fraction of λ Boo stars are located within the classical δ Sct/γ Dor instability strip. Paunzen et al. (2002) presented a detailed analysis of their pulsational behaviour, based on ground-based photometry. They concluded that at least 70 per cent of the group members inside the classical instability strip pulsate, and they

★ E-mail: simon.murphy@sydney.edu.au

do so with high overtone p modes ($Q < 0.020$ d). This group of stars is perfectly suited to test pulsational models of stars with non-solar atmospheric composition. Recent advances in determining precise MS ages of γ Dor stars from asteroseismology offer a reciprocal benefit (Kurtz et al. 2014; Saio et al. 2015).

An opportunity to re-evaluate the evolutionary status of λ Boo stars has arrived with *Gaia* Data Release 1 (DR1; Gaia Collaboration et al. 2016; Lindegren et al. 2016), which has added heavily to the number of λ Boo stars with precise parallaxes. We examine an updated HR diagram of these stars in an attempt to decipher the enigma surrounding their peculiarities. In Section 2, we describe our data extraction procedures. The HR diagram is described in Section 3 and interpreted in Section 4, then brief conclusions are given in Section 5.

2 DATA EXTRACTION

The starting point of our target selection was the catalogue of bona fide λ Boo stars by Murphy et al. (2015). From this sample, we made two selections. First, we selected objects for which parallaxes with an error smaller than 25 per cent in the *Hipparcos* catalogue (van Leeuwen 2007) and/or *Gaia* DR1 (Gaia Collaboration et al. 2016) are available. Most of the parallaxes are much smaller than 25 per cent, as we discuss in Section 2.2. Secondly, we included only those stars with available Johnson *UBV*, Strömgren–Crawford *uvbyβ* and Geneva 7-colour photometry, taken from Paunzen (2015) and the General Catalogue of Photometric Data (GCPD[1]). Where possible, averaged and weighted mean values were used throughout. The final sample consists of 172 stars.

2.1 Colours and reddening

Throughout this analysis, the following relation between extinction, A, and colour excess (reddening), E, in specific bands, is used

$$A_V = 3.1E_{(B-V)} = 4.3E_{(b-y)} = 4.95E_{(B2-V1)}.$$

The reddening for the targets was estimated using photometric calibrations in the Strömgren *uvbyβ* (Crawford 1978, 1979) and the Q-parameter within the Johnson *UBV* system (Johnson 1958). These methods are based only on photometric indices and do not take any distance estimates via parallax measurements into account. In addition, for all stars, the distance (derived from the parallaxes) and Galactic coordinates were used to determine the reddening from the Amôres & Lépine (2005) extinction model. If several estimates were available, they were compared and were always in excellent agreement.

The effective temperatures ($T_{\rm eff}$) of the individual stars were calibrated by using the measurements in the Johnson *UBV*, Geneva 7-colour and Strömgren–Crawford *uvbyβ* photometric systems (Golay 1974). This approach was chosen because it yields the most homogeneous result; taking $T_{\rm eff}$ values from the literature, e.g. from spectroscopy, introduces a variety of unknown biases (Lebzelter et al. 2012), such as the use of different stellar atmosphere models, spectral resolutions, analytic methods and so on. Here, we used the following calibrations for the three photometric systems:

(i) Johnson *UBV*: Paunzen, Schnell & Maitzen (2005, 2006).

(ii) Geneva 7-colour: Kunzli et al. (1997), Paunzen et al. (2005, 2006).

(iii) Strömgren–Crawford *uvbyβ*: Moon & Dworetsky (1985), Napiwotzki, Schoenberner & Wenske (1993), Balona (1994), Ribas et al. (1997) and Paunzen et al. (2005, 2006).

The individual $T_{\rm eff}$ values within each photometric system were first checked for intrinsic consistency and then averaged. The error of the photometric measurements in the used systems for our targets are normally below 0.01 mag. Kunzli et al. (1997) investigated in detail, the influence of the observational errors on the $T_{\rm eff}$ estimates, finding the dispersion and systematic zero-point shifts to be small. These final $T_{\rm eff}$ values, together with the standard deviations of the means, are listed in Table A1. Also given there are the absolute and apparent magnitudes ($M_{\rm V}$, $m_{\rm V}$) of each star, calculated using their parallax measurements (π) by applying the basic formula

$$M_{\rm V} = m_{\rm V} + 5\,(\log\pi + 1) - A_{\rm V}. \quad (1)$$

We used the $m_{\rm V}$ values given by Kharchenko (2001), who transformed the Tycho data uniformly to the Johnson system. This is the most homogeneous sample available for this data type.

Finally, the bolometric correction (B.C.) for a given $T_{\rm eff}$ was derived using the relation by Flower (1996).

For the error estimate of $\log L$, only the error of the parallax was taken into account. The mean error of the mean extinctions ($\overline{\sigma_A}$) is 0.01 mag, which propagates to an error contribution of 0.004 dex for the final luminosities. The B.C. for A stars is very flat. It ranges from $+0.03$ to -0.06 mag for $7000 < T_{\rm eff} < 9000$ K. Even a $T_{\rm eff}$ error of 30 per cent results in a B.C. error contribution to the luminosity of 0.006 dex.

2.2 Parallax validation

Where both *Gaia* and *Hipparcos* parallaxes were available, we used the measurement with the smallest uncertainty.

Fig. 1a shows the comparison of the absolute magnitudes derived from the *Hipparcos* and *Gaia* DR1, respectively. No significant offset for the 69 stars in common has been detected: $\Delta\overline{M_{\rm V}} = +0.05 \pm 0.41$ mag.

Three stars (HD 21335, HD 105058 and HD 114930) were found to have a $\Delta\overline{M_{\rm V}}$ value that is 2σ larger than calculated from the individual errors. From these, HD 21335 and HD 105058 are listed as visual and/or spectroscopic binary systems in the Washington Visual Double Star Catalog (Mason et al. 2001) and/or by Faraggiana et al. (2004). Parallax measurements for binaries already encountered difficulties in the *Hipparcos* era (Mason et al. 1999), with very erratic parallaxes being obtained for several systems, depending on the separation and magnitude difference of the components. The behaviour of the *Gaia* measurements in this respect is still to be investigated in detail. For HD 114930 ($\Delta M_{\rm V} = +0.84$ mag), we have found no plausible explanation for the large differences. Since for this object, the *Gaia* parallax has the smaller fractional parallax uncertainty [$f_{\rm G} = \sigma_{\rm G}(\pi)/\pi = 6.7$ per cent], this is the one we used. The *Hipparcos* fractional parallax uncertainty is unusually large ($f_{\rm H} = 15.3$ per cent). The distribution of f is shown in Fig. 1b.

A systematic bias occurs when using parallax-limited samples (Trumpler & Weaver 1953), which on average leads to the overestimation of stellar distances. Lutz & Kelker (1973) calculated corrections for the resulting bias in the absolute magnitudes of individual stars. Their correction reaches 0.43 mag for $f = 17.5$ per cent. However, since the publication of the *Hipparcos* data, a debate has emerged on the appropriateness of this correction for single stars (Smith 2003; Francis 2014). On the basis of Monte Carlo

[1] http://gcpd.physics.muni.cz/

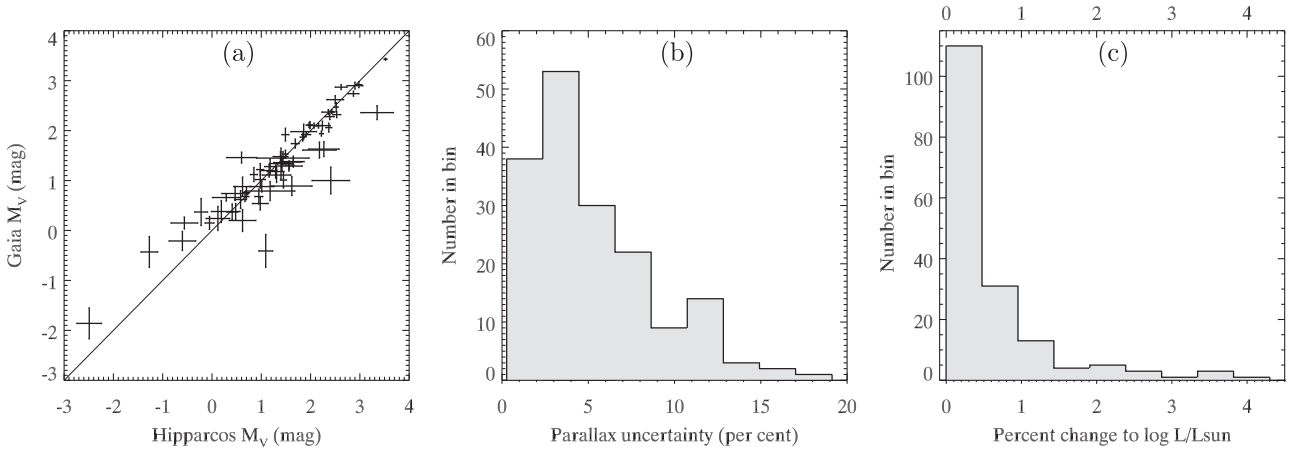

Figure 1. (a) A comparison of the absolute magnitudes derived from the parallaxes of *Hipparcos* and *Gaia* DR1, showing no obvious offset. The diagonal line represents $M_{V,\,Gaia} = M_{V,\,Hip}$. (b) The distribution of fractional parallax uncertainties, f. Where both *Gaia* and *Hipparcos* parallaxes were available, we used the one having the smaller uncertainty; 86 per cent of our sample have $f < 10$ per cent. (c) Distribution of the percentage change in $\log L/L_\odot$ that would result if a Lutz–Kelker correction (equation 2) were applied. We applied no such correction. Note that the vertical scales of (b) and (c) differ.

simulations, Francis (2014) showed that the overall (net) correction for the absolute magnitude can be described as

$$\Delta(M_V) = -5.35 \left(\frac{\sigma(\pi)}{\pi} \right)^2, \quad (2)$$

but he also wrote 'there is, in practice, no circumstance in which the (Lutz–Kelker) correction should be applied'.

That is not to say that no bias exists, rather, that the Lutz–Kelker correction is not the appropriate treatment. A full Bayesian treatment is preferred but not straightforward, especially for $f > 0.2$, since it requires the difficult selection of an appropriate prior (Bailer-Jones 2015).

In this work, we have calculated the numerical correction for each star according to equation (2) to evaluate its significance. We found the resulting correction to our logarithmic luminosities to be smaller than 1 per cent for 82 per cent of our sample (Fig. 1c). In no case does this correction exceed the 1σ uncertainty in $\log L$. We therefore deemed the correction insignificant, and made no correction to our data.

It is useful to compare literature estimates of the significance of bias corrections for similar stellar populations. The sample of 90 Mount Wilson Subgiants (Adams et al. 1935) is particularly useful here, having comparable absolute magnitudes, dispersion and fractional parallax uncertainties to our λ Boo stars. Sandage, Beaton & Majewski (2016) applied the Sandage & Saha (2002) treatment of bias to the Mount Wilson Subgiants, and also found the resulting corrections to be insignificant.

3 THE HR DIAGRAM

Fig. 2 shows the selected λ Boo stars and candidates on an HR diagram, colour-coded by membership status. We have added evolutionary tracks at $Z = 0.02$, calculated with time-dependent convection (TDC) models of mixing length $\alpha_{MLT} = 1.8\ h_p$ (pressure scaleheights) from Grigahcène et al. (2005). This value of α_{MLT} was empirically validated by matching the observed and theoretical instability strips for δ Sct and γ Dor stars (Dupret et al. 2005). We have included those same theoretical instability strips, which were computed for the radial modes for the δ Sct stars, and $\ell = 1$ modes for the γ Dor stars.

The global metallicity of these models, Z, is higher than the measured metallicity of λ Boo stars, which deserves some discussion. The chemical peculiarities of λ Boo stars are believed to be limited to the surface, so TDC models with a global metallicity typical of A stars in the Galactic plane were chosen. Generally, metal-poor stars are hotter and less luminous than metal-rich stars of the same mass and age due to differences in the opacity. While we expect no large systematic displacement of the λ Boo stars in Fig. 2 with respect to the evolutionary tracks, any displacement of these stars that does occur will be to the lower left. This is one potential explanation of some objects that lie below the ZAMS. Other explanations include underestimated extinction, particularly because objects at the ZAMS are located in or near star formation regions (e.g. two objects that are in the Orion OB1 association), or technical problems with the *Gaia* parallaxes in the first data release due to undetected binaries (Lindegren et al. 2016).

3.1 Influence on pulsation

The fact that the low surface metallicity is attributed to the accretion of material with a low dust-to-gas mass ratio has strong implications on the driving of pulsation. The pressure-mode (p mode) oscillations of δ Sct stars are driven by the opacity mechanism operating on the He II partial ionization zone. Murphy (2014) argued that the delivery of fresh helium at the surface, combined with the typically rapid rotation of λ Boo stars, acts to prevent helium from gravitationally settling in these stars. The driving zone is therefore well stocked with helium, which Murphy (2014) argued would lead to stronger oscillation amplitudes in these stars, and/or a higher fraction of them being pulsators, compared to an otherwise identical sample of chemically normal stars. We have therefore collated pulsation properties from the literature (Antonello & Mantegazza 1982; Paunzen et al. 1997, 1998, 2002, 2014, 2015).

Fig. 3 shows the pulsation properties of members and probable members of the λ Boo class. There are 16 (38 per cent) non-pulsating λ Boo stars in the instability strip, at the photometric precision achieved in ground-based surveys (typically a few mmag). *Kepler* observations have shown that many δ Sct stars have oscillation amplitudes below 1 mmag, so these objects are readily explained as variables for which the photometry was insufficiently sensitive to detect the oscillations. Three pulsating stars are much hotter than

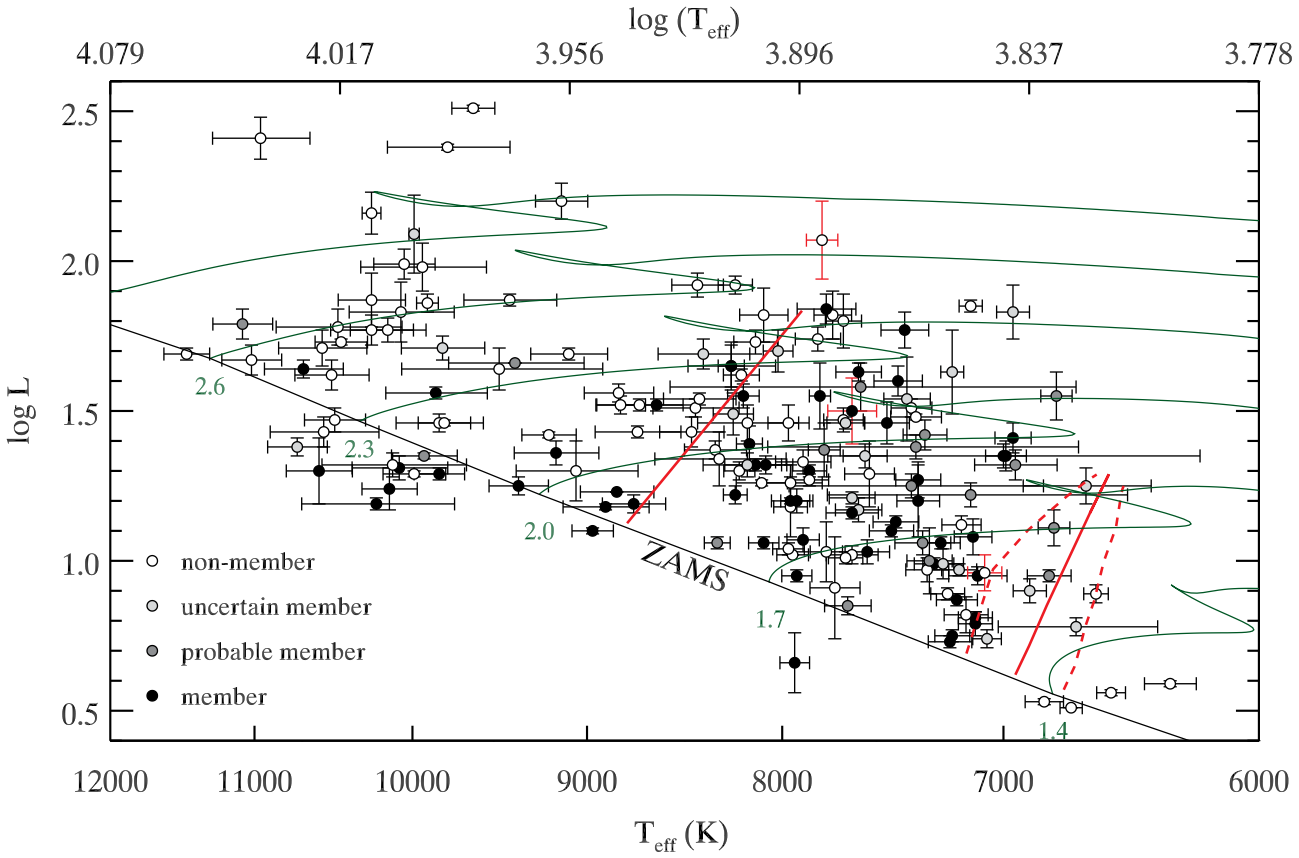

Figure 2. An HR diagram of 172 λ Boo stars and candidates with *Hipparcos* or *Gaia* parallaxes. The probability of membership in the λ Boo class is indicated by symbol shade. Evolutionary tracks at $Z = 0.02$ are shown as green lines, with their corresponding masses (in $M_{\odot}$) written beneath the ZAMS (black line). The δ Sct and γ Dor instability strips are delimited with solid and dashed red lines, respectively. The temperature scale is logarithmic. The three stars with anomalously large $\Delta\overline{M_V}$ are shown with red error bars.

the instability strip. In the following, the characteristics of these objects plus the δ Sct star well below the ZAMS are discussed in more detail.

HD 87271. The Strömgren–Crawford indices are the following: $(b - y) = +0.151$ mag, $m_1 = +0.094$ mag, $c_1 = +0.939$ mag and $\beta = 2.775$ mag. Those are not self-consistent (Crawford 1978, 1979). If we assume that the reddening is zero, leading to $T_{\rm eff} \sim 7500$ K, then the c_1 index is much too high for an MS star. On the other hand, the β index is not consistent with a hotter MS object. A detailed spectroscopic analysis is required for definitive characterization.

HD 172167 (Vega). The variability of this bright standard star has been extensively reviewed by Butkovskaya (2014). It seems to vary on time-scales typical for classical pulsation up to several decades indicating similarities to the solar cycle. The membership to the λ Boo group has been extensively discussed by Murphy et al. (2015).

HD 183324. Spectroscopically determined values of $T_{\rm eff}$ (Heiter et al. 1998) are in good agreement with our photometrically derived one. It has a very short period (30 min) and a very low surface metallicity ($Z = -1.5$ dex). Therefore, HD 183324 seems to be quite outstanding compared to the other pulsating λ Boo stars. Gerbaldi, Faraggiana & Lai (2003) reported that the radial velocity is variable but they were not able to detect any optical companion using speckle interferometry. This variability could be caused, other than by pulsation, by undetected binarity, which would explain the location below the ZAMS.

HD 290799. This star is a member of the Orion OB1 association (Gray & Corbally 1993). The estimated reddening of 0.022 mag is low for this region. Paunzen et al. (2002) estimated $M_V = +2.62 \pm 0.30$ mag on the basis of photometric data and the distance to the Orion OB1 association, only. This value is about 0.5 mag brighter than our estimate and would put HD 290799 on the ZAMS. There are no Geneva colours available, which prevents us from checking the intrinsic consistency of the Strömgren–Crawford ones. Therefore, we are not able to resolve the inconsistency for HD 290799.

Asteroseismology is a promising tool to assess whether the metal depletion in λ Boo stars is global or limited to the surface instead. A detailed analysis with ultraprecise *Kepler* (and later, *TESS*) light curves is highly warranted, and will be the subject of future work.

4 DISCUSSION

The distribution of λ Boo stars on the HR diagram appears divided loosely around the classical (δ Sct) instability strip. On the upper MS, which we define as the region hotter than the blue edge of the instability strip, the λ Boo stars are confined to the ZAMS. However, within the instability strip, the λ Boo stars occupy a wide range of MS ages, with some possibly above the terminal-age main-sequence (TAMS). Redward of the instability strip, no λ Boo stars are observed.

It is not clear whether this distribution is to be explained in terms of the physics operating at different effective temperatures, or at

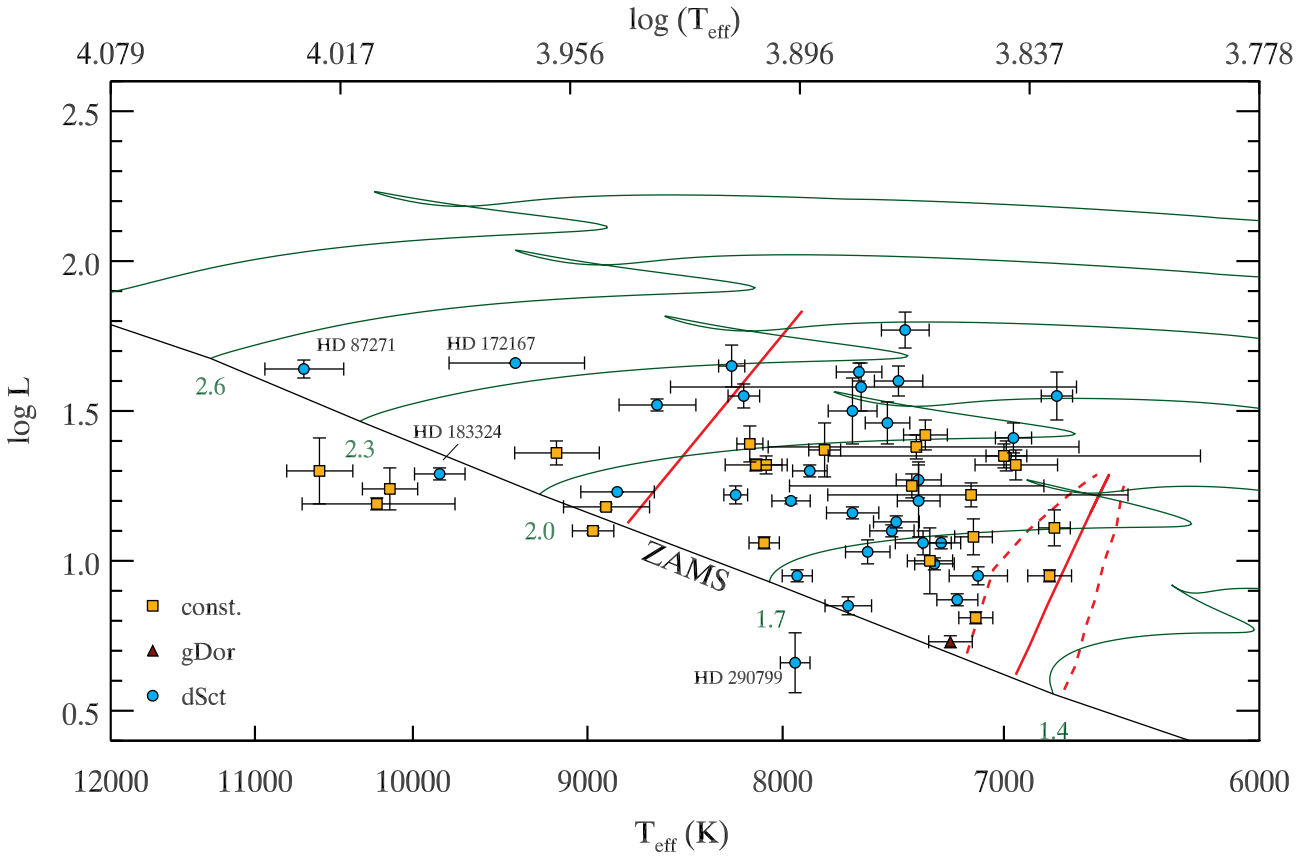

Figure 3. As Fig. 2, but showing only the 52 members and 17 probable members of the λ Boo class. Different symbol types show the pulsation properties. Constant stars show no variability greater than a few mmag. The one γ Dor star is HR 8799 (Gray & Kaye 1999). Stars labelled with HD numbers are discussed in the text.

different masses instead. Its division around the instability strip is coincidental, particularly since not all group members are observed to pulsate, and the δ Sct hot edge is clearly not a hard boundary beyond which all λ Boo stars are confined to the ZAMS.

In the coolest stars, the weaker radiation field is least efficient at preventing the accretion of dust, so the composition of any accreted material is not highly anomalous to begin with. Further, the surface convection zone is deep and massive enough that any accreted material is thoroughly mixed and a large contamination is required before peculiarities are observed.

In the hottest stars the radiation field is strongest, and the quantity of material required to pollute the surface is lower, but neither of these principles has resulted in more λ Boo stars towards the TAMS. Thus, the confinement of λ Boo stars to the ZAMS indicates that the phenomenon is associated with star formation in some way. In what follows, we reconcile the observations with current theory.

There are several different hypotheses surrounding the development of λ Boo peculiarities, each with their own merits. All of these hypotheses are related to dust-gas separation and the accretion of dust-depleted material, with two notable exceptions: (i) the refuted composite-spectrum hypothesis, which was covered in Section 1, and has been more comprehensively reviewed by Murphy et al. (2015); and (ii) the diffusion and mass-loss mechanism (Michaud & Charland 1986), which tends to produce overabundances of Fe-peak elements typical of Am stars (Vick et al. 2010, 2011), rather than the underabundances observed in λ Boo stars. We suggest that it is not a single mechanism that is responsible, but that several channels can form λ Boo spectra under certain conditions.

We start with the hot ZAMS λ Boo stars. Approximately half of the Herbig Ae/Be (HAeBe) stars show abundance patterns in common with λ Boo stars (Folsom et al. 2012). It is possible that stars begin their MS lives with this chemical imprint of star formation, resulting from partial accretion of the protoplanetary disc. Kama et al. (2015) suggested that jovian planets can exaggerate the process by trapping dust in the disc. Particularly for massive stars, the protoplanetary disc is short-lived (Ribas, Bouy & Merín 2015), and rapid rotation mixes these stars on short time-scales (e.g. Maeder & Meynet 2000; Espinosa Lara & Rieutord 2013), so the peculiarities disappear shortly after the stars begin hydrogen fusion, therefore the phenomenon is limited to the ZAMS.

At lower masses, the λ Boo phenomenon is observed across the whole MS phase, so the accretion of protoplanetary material cannot be the sole explanation. An alternative is that the gas-rich material causing the peculiarities has been ablated from hot Jupiters (Jura 2015). The idea has support from observations that A stars are efficient at forming high-mass planets (Johnson et al. 2011; Murphy, Bedding & Shibahashi 2016), and some are observed in small orbits (Collier Cameron et al. 2010). The trapping of material in a planetary reservoir allows the accretion episode to be delayed, which accounts for the older λ Boo stars. The rather abrupt termination in λ Boo stars as a function of mass, seen in Fig. 2, is also explained by this mechanism. The peak of the planet occurrence rate distribution, as a function of host-star mass, has a sharp cut-off at the high-mass end: $1.9^{+0.1}_{-0.5}$ $M_{\odot}$ (Reffert et al. 2015). Only around 23 per cent of λ Boo stars have an infrared excess (Paunzen et al. 2003), so a further strength of this mechanism is that it does not demand one.

The hot-Jupiter hypothesis is not perfect – it cannot explain the lack of λ Boo stars in certain cluster environments. Gray & Corbally (2002) assessed 220 stars in intermediate-age (35–830 Myr) clusters, for which cluster membership was certain and no bias for or against the detection of λ Boo peculiarity was known. Not a single λ Boo star was found. For *field* λ Boo stars, they estimated the occurrence rate to be 2.0–2.5 per c'ent of the population. Applying a binomial distribution to their results for clusters at the field occurrence rate of 2.0 per cent, we find the probability of detecting zero λ Boo stars, $P(X = 0) = 0.012$. This statistically significant result is not explained by the hot-Jupiter hypothesis, given that such planets have no difficulty forming in clusters (Lovis & Mayor 2007; Sato et al. 2007; Quinn et al. 2012; Meibom et al. 2013).

The lack of λ Boo stars in intermediate-age clusters is explained if the dominant source of accreted material is diffuse ISM clouds (Martínez-Galarza et al. 2009), because such clouds are not observed in clusters. The diffuse ISM hypothesis is also capable of explaining the lack of λ Boo stars in the later MS phases of more massive stars, since their shorter lifetimes reduce the chances of encountering an ISM cloud after leaving their stellar nursery. In fact, none of the aforementioned observations are incompatible with the ISM accretion model, but it is not without problems. The star δ Vel has been presented as a cast-iron example of an object interacting with the ISM but it does not belong to the λ Boo class (Gáspár et al. 2008). Confirmed interactions with the ISM are rare, particularly in the local bubble where most λ Boo stars are found but interstellar gas is deficient (Lallement et al. 2003), whereas several A stars with resolved debris discs are known (Booth et al. 2013). While Martínez-Galarza et al. (2009) conceded that their models of infrared excesses for A stars fitted debris discs just as well as the interactions with the ISM they were promoting, Draper et al. (2016) have found infrared emission around 9 λ Boo stars that is *only* consistent with debris discs. There are also observational concerns that the ISM accretion rates required for λ Boo peculiarities are unachievable (Jura 2015).

Finally, we note that there are many more λ Boo stars on the ZAMS for the hotter half of the sample in Fig. 2 than for the cooler half. This is explained by selection effects. For instance, pre-MS stars have often been targets in the search for λ Boo stars (Acke & Waelkens 2004; Folsom et al. 2012), and the majority of known pre-MS A stars lie at the hotter end of the temperature range of Fig. 2. The latter is easily seen in catalogues of stellar spectral types. Of the 150 stars with spectral types of A[0-9]e in the Skiff (2014) catalogue, 102 (68 per cent) have spectral types of A2e or earlier.

5 CONCLUSIONS

The location of λ Boo stars on an HR diagram suggests there is more than one channel by which accretion may cause λ Boo peculiarities in stellar spectra. We propose this as the reason that a single formation channel has not been agreed upon after decades of attempts. The relative importance of the different channels varies with age, temperature and environment (cluster versus field).

Young stars form λ Boo-like spectra via accretion of a protoplanetary disc, with dust-gas separation being more efficient if giant planets are present. Older stars may accrete gas ablated from hot Jupiters, but the absence of λ Boo stars in intermediate-age clusters suggests this cannot be the sole mechanism forming these peculiarities. Interaction with diffuse clouds in the ISM has strong theoretical basis, but is also not the dominant mechanism according to observations of debris discs around λ Boo stars, and of ISM accretion rates on to other stars.

The future of λ Boo research is divided between further observations and computative analyses. Quantitative modelling, considering all channels forming λ Boo-like spectra, is highly sought after. A homogeneous investigation of the infrared properties of class members can further pin-down the source of dust. And finally, asteroseismology will probe the penetrative depth of the metal depletion.

ACKNOWLEDGEMENTS

We thank J. Molenda-Żakowicz for discussion on the paper. This research was supported by the Australian Research Council. Funding for the Stellar Astrophysics Centre is provided by The Danish National Research Foundation (grant agreement no.: DNRF106). This work has made use of data from the European Space Agency (ESA) mission *Gaia* (http://www.cosmos.esa.int/gaia), processed by the *Gaia* Data Processing and Analysis Consortium (DPAC, http://www.cosmos.esa.int/web/gaia/dpac/consortium). Funding for the DPAC has been provided by national institutions, in particular the institutions participating in the *Gaia* Multilateral Agreement. This research has made use of the Washington Double Star Catalog maintained at the US Naval Observatory.

REFERENCES

Abt H. A., Morrell N. I., 1995, ApJS, 99, 135
Acke B., Waelkens C., 2004, A&A, 427, 1009
Adams W. S., Joy A. H., Humason M. L., Brayton A. M., 1935, ApJ, 81, 187
Amôres E. B., Lépine J. R. D., 2005, AJ, 130, 659
Andrievsky S. M. et al., 2002, A&A, 396, 641
Antonello E., Mantegazza L., 1982, A&AS, 49, 709
Bailer-Jones C. A. L., 2015, PASP, 127, 994
Balona L. A., 1994, MNRAS, 268, 119
Baschek B., Slettebak A., 1988, A&A, 207, 112
Booth M. et al., 2013, MNRAS, 428, 1263
Butkovskaya V. V., 2014, Bull. Crimean Astrophys. Obs., 110, 80
Collier Cameron A. et al., 2010, MNRAS, 407, 507
Crawford D. L., 1978, AJ, 83, 48
Crawford D. L., 1979, AJ, 84, 1858
Draper Z. H., Matthews B. C., Kennedy G. M., Wyatt M. C., Venn K. A., Sibthorpe B., 2016, MNRAS, 456, 459
Dupret M., Grigahcène A., Garrido R., Gabriel M., Scuflaire R., 2005, A&A, 435, 927
Espinosa Lara F., Rieutord M., 2013, A&A, 552, A35
Faraggiana R., Bonifacio P., 1999, A&A, 349, 521
Faraggiana R., Gerbaldi M., Bonifacio P., 2001, A&A, 380, 286
Faraggiana R., Bonifacio P., Caffau E., Gerbaldi M., Nonino M., 2004, A&A, 425, 615
Flower P. J., 1996, ApJ, 469, 355
Folsom C. P., Bagnulo S., Wade G. A., Alecian E., Landstreet J. D., Marsden S. C., Waite I. A., 2012, MNRAS, 422, 2072
Francis C., 2014, MNRAS, 444, L6
Gaia Collaboration et al., 2016, A&A, 595, A2
Gáspár A., Su K. Y. L., Rieke G. H., Balog Z., Kamp I., Martínez-Galarza J. R., Stapelfeldt K., 2008, ApJ, 672, 974
Gerbaldi M., Faraggiana R., Lai O., 2003, A&A, 412, 447
Golay M., ed., 1974, Astrophysics and Space Science Library, Vol. 41, Introduction to Astronomical Photometry. Kluwer, Dordrecht, p. 375+
Gray R. O., Corbally C. J., 1993, AJ, 106, 632
Gray R. O., Corbally C. J., 1998, AJ, 116, 2530
Gray R. O., Corbally C. J., 2002, AJ, 124, 989
Gray R. O., Kaye A. B., 1999, AJ, 118, 2993

Griffin R. E., Gray R. O., Corbally C. J., 2012, A&A, 547, A8
Grigahcène A., Dupret M.-A., Gabriel M., Garrido R., Scuflaire R., 2005, A&A, 434, 1055
Heiter U., Kupka F., Paunzen E., Weiss W. W., Gelbmann M., 1998, A&A, 335, 1009
Holweger H., Sturenburg S., 1993, in Dworetsky M. M., Castelli F., Faraggiana R., eds, ASP Conf. Ser. Vol. 44, IAU Colloq. 138: Peculiar versus Normal Phenomena in A-type and Related Stars. Astron. Soc. Pac., San Francisco, p. 356
Iliev I. K., Barzova I. S., 1995, A&A, 302, 735
Iliev I. K., Paunzen E., Barzova I. S., Griffin R. F., Kamp I., Claret A., Koen C., 2002, A&A, 381, 914
Johnson H. L., 1958, Lowell Obs. Bull., 4, 37
Johnson J. A. et al., 2011, ApJS, 197, 26
Jura M., 2015, AJ, 150, 166
Kama M., Folsom C. P., Pinilla P., 2015, A&A, 582, L10
Kamp I., Paunzen E., 2002, MNRAS, 335, L45
Kamp I., Iliev I. K., Paunzen E., Pintado O. I., Solano E., Barzova I. S., 2001, A&A, 375, 899
Kharchenko N. V., 2001, Kinematika Fiz. Nebesnykh Tel, 17, 409
Kunzli M., North P., Kurucz R. L., Nicolet B., 1997, A&AS, 122, 51
Kurtz D. W., Saio H., Takata M., Shibahashi H., Murphy S. J., Sekii T., 2014, MNRAS, 444, 102
Lallement R., Welsh B. Y., Vergely J. L., Crifo F., Sfeir D., 2003, A&A, 411, 447
Lebzelter T. et al., 2012, A&A, 547, A108
Lindegren L. et al., 2016, A&A, 595, A4
Lovis C., Mayor M., 2007, A&A, 472, 657
Lutz T. E., Kelker D. H., 1973, PASP, 85, 573
Maeder A., Meynet G., 2000, ARA&A, 38, 143
Martínez-Galarza J. R., Kamp I., Su K. Y. L., Gáspár A., Rieke G., Mamajek E. E., 2009, ApJ, 694, 165
Mason B. D. et al., 1999, AJ, 117, 1890
Mason B. D., Wycoff G. L., Hartkopf W. I., Douglass G. G., Worley C. E., 2001, AJ, 122, 3466
Meibom S. et al., 2013, Nature, 499, 55
Michaud G., Charland Y., 1986, ApJ, 311, 326
Moon T. T., Dworetsky M. M., 1985, MNRAS, 217, 305
Murphy S. J., 2014, PhD thesis, Univ. Central Lancashire
Murphy S. J. et al., 2015, Publ. Astron. Soc. Aust., 32, 36
Murphy S. J., Bedding T. R., Shibahashi H., 2016, ApJ, 827, L17
Napiwotzki R., Schoenberner D., Wenske V., 1993, A&A, 268, 653
Paunzen E., 1997, A&A, 326, L29
Paunzen E., 2001, A&A, 373, 633
Paunzen E., 2015, A&A, 580, A23
Paunzen E., Kuschnig R., Handler G., Gelbmann M., Weiss W. W., 1997, A&AS, 124, 23
Paunzen E., Weiss W. W., Martinez P., Matthews J. M., Pamyatnykh A. A., Kuschnig R., 1998, A&A, 330, 605
Paunzen E. et al., 2002, A&A, 392, 515
Paunzen E., Kamp I., Weiss W. W., Wiesemeyer H., 2003, A&A, 404, 579
Paunzen E., Schnell A., Maitzen H. M., 2005, A&A, 444, 941
Paunzen E., Schnell A., Maitzen H. M., 2006, A&A, 458, 293
Paunzen E., Skarka M., Holdsworth D. L., Smalley B., West R. G., 2014, MNRAS, 440, 1020
Paunzen E., Skarka M., Walczak P., Holdsworth D. L., Smalley B., West R. G., Janík J., 2015, MNRAS, 453, 1241
Quinn S. N. et al., 2012, ApJ, 756, L33
Reffert S., Bergmann C., Quirrenbach A., Trifonov T., Künstler A., 2015, A&A, 574, A116
Ribas Á., Bouy H., Merín B., 2015, A&A, 576, A52
Ribas I., Jordi C., Torra J., Gimenez A., 1997, A&A, 327, 207
Saio H., Kurtz D. W., Takata M., Shibahashi H., Murphy S. J., Sekii T., Bedding T. R., 2015, MNRAS, 447, 3264
Sandage A., Saha A., 2002, AJ, 123, 2047
Sandage A., Beaton R. L., Majewski S. R., 2016, PASP, 128, 064202
Sato B. et al., 2007, ApJ, 661, 527
Skiff B. A., 2014, VizieR Online Data Catalog, 1
Smith H., 2003, MNRAS, 338, 891
Stütz C., Paunzen E., 2006, A&A, 458, L17
Trumpler R. J., Weaver H. F., 1953, Statistical Astronomy. Dover Publications, New York
Turcotte S., 2002, ApJ, 573, L129
Turcotte S., Charbonneau P., 1993, ApJ, 413, 376
van Leeuwen F., 2007, A&A, 474, 653
Venn K. A., Lambert D. L., 1990, ApJ, 363, 234
Vick M., Michaud G., Richer J., Richard O., 2010, A&A, 521, A62
Vick M., Michaud G., Richer J., Richard O., 2011, A&A, 526, A37
Waters L. B. F. M., Trams N. R., Waelkens C., 1992, A&A, 262, L37

APPENDIX

Table A1. Parameters for the 172 λ Boo stars and candidates considered in this work, with *Hipparcos* ('Hip') or *Gaia* parallaxes. Membership probability ('mem.') in the λ Boo class (from Murphy et al. 2015) is indicated with integers between 1 and 4, with 1 being certain members and 4 being non-members. B.C. stands for bolometric correction, and other symbols have their usual usage as described in the text. Where absolute magnitudes are missing, no parallax was available in that survey. The final column gives the variability type from sources described in Section 3.1.

HD	HIP/TYC	mem.	m_V (mag)	A_V (mag)	B.C. (mag)	T_{eff} (K)	$M_{V,\,Hip}$ (mag)	$M_{V,\,Gaia}$ (mag)	$\log L/L_\odot$	var?
3	424	3	6.685	0.000	+0.01	8390 ± 232	+0.98 ± 0.16	+0.54 ± 0.13	1.69 ± 0.05	–
319	636	1	5.931	0.012	+0.02	8080 ± 77	+1.45 ± 0.06	+1.01 ± 0.16	1.32 ± 0.03	const.
2904	2628	3	6.406	0.023	−0.21	9820 ± 247	+0.48 ± 0.09	+0.38 ± 0.16	1.71 ± 0.04	–
4158	5849–1699–1	1	9.536	0.577	+0.03	7820 ± 50	–	+0.88 ± 0.27	1.55 ± 0.11	–
6173	3271–1475–1	3	8.520	0.490	−0.25	9990 ± 31	–	−0.46 ± 0.31	2.09 ± 0.13	–
6870	5321	1	7.473	0.000	+0.03	7300 ± 87	+2.39 ± 0.09	+2.28 ± 0.06	0.99 ± 0.02	δ Sct
7908	6108	1	7.304	0.000	+0.03	7120 ± 73	+2.87 ± 0.11	+2.74 ± 0.05	0.81 ± 0.02	const.
9100	6981	4	6.013	0.000	+0.03	7760 ± 88	+0.19 ± 0.20	+0.38 ± 0.22	1.82 ± 0.08	δ Sct
11413	8593	1	5.933	0.007	+0.02	7870 ± 82	+1.49 ± 0.05	+1.53 ± 0.08	1.30 ± 0.02	δ Sct
11503	8832	4	4.598	0.018	−0.35	10480 ± 193	+1.07 ± 0.10	–	1.47 ± 0.04	other
13755	10304	1	7.829	0.000	+0.03	6990 ± 86	+1.65 ± 0.22	+1.38 ± 0.11	1.35 ± 0.05	δ Sct
15164	635–338–1	1	8.281	0.000	+0.03	7120 ± 73	–	+2.77 ± 0.10	0.79 ± 0.04	–
16811	12640	4	5.735	0.060	−0.28	10150 ± 232	+0.34 ± 0.09	–	1.77 ± 0.04	–
16955	12744	4	6.376	0.000	0.00	8450 ± 164	+1.29 ± 0.17	+1.18 ± 0.13	1.43 ± 0.05	–
17138	13133	2	6.262	0.042	+0.01	8320 ± 65	+2.16 ± 0.05	+2.10 ± 0.05	1.06 ± 0.02	other
21335	16077	4	6.530	0.001	+0.03	7810 ± 74	+1.09 ± 0.14	−0.41 ± 0.33	2.07 ± 0.13	–
22470	16803	4	5.236	0.000	−1.13	14350 ± 238	−0.63 ± 0.17	–	2.15 ± 0.07	other
23258	17453	1	6.076	0.000	−0.13	9380 ± 168	+1.62 ± 0.07	–	1.25 ± 0.03	–
23392	17462	1	8.246	0.163	−0.28	10140 ± 169	–	+1.65 ± 0.17	1.24 ± 0.07	const.
24472	18153	2	7.097	0.000	+0.02	6810 ± 90	+2.36 ± 0.13	+2.37 ± 0.05	0.95 ± 0.02	const.
24712	18339	4	5.984	0.000	+0.03	7240 ± 74	+2.52 ± 0.04	+2.47 ± 0.09	0.89 ± 0.02	other
27404	20262	4	7.931	0.127	+0.03	7590 ± 114	+1.26 ± 0.47	+1.51 ± 0.28	1.29 ± 0.11	other
30422	22192	1	6.173	0.000	0.02	7930 ± 72	+2.43 ± 0.04	+2.38 ± 0.04	0.95 ± 0.02	δ Sct
30739	22509	4	4.348	0.073	−0.14	9430 ± 264	+0.09 ± 0.06	–	1.87 ± 0.02	–
31293	22910	4	7.064	0.035	+0.02	8170 ± 249	+1.31 ± 0.29	+1.11 ± 0.15	1.46 ± 0.06	other
31295	22845	1	4.646	0.088	−0.05	8900 ± 231	+1.80 ± 0.02	–	1.18 ± 0.01	const.
34787	25197	4	5.236	0.058	−0.23	9910 ± 65	+0.11 ± 0.07	–	1.86 ± 0.03	–
34797	24827	4	6.505	0.039	−1.05	13860 ± 176	−0.48 ± 0.23	–	2.09 ± 0.09	other
35242	25205	1	6.330	0.000	+0.02	8230 ± 59	+1.69 ± 0.08	+1.74 ± 0.09	1.22 ± 0.03	δ Sct
36496	26410	3	6.302	0.016	0.03	7640 ± 107	+1.83 ± 0.09	–	1.17 ± 0.04	–
37886	4771–343–1	4	9.005	0.197	−0.78	12490 ± 54	–	+0.96 ± 0.24	1.52 ± 0.10	–
38545	27316	4	5.717	0.000	+0.02	8250 ± 218	+0.63 ± 0.19	–	1.65 ± 0.08	const.
39283	27949	4	4.960	0.108	−0.08	9100 ± 211	+0.53 ± 0.04	–	1.69 ± 0.02	–
39421	27713	3	5.954	0.000	+0.02	8240 ± 100	+0.98 ± 0.10	+1.02 ± 0.17	1.49 ± 0.07	–
40588	28517	1	6.182	0.114	−0.03	8750 ± 167	+1.78 ± 0.07	–	1.19 ± 0.03	–
42503	29159	1	7.434	0.000	+0.03	7460 ± 109	+0.47 ± 0.27	+0.74 ± 0.14	1.60 ± 0.05	δ Sct
47152	31737	4	5.743	0.129	−0.37	10560 ± 281	+0.48 ± 0.14		1.71 ± 0.06	other
54272	1353–663–1	3	8.774	0.167	+0.03	6890 ± 69		+2.51 ± 0.09	0.90 ± 0.04	γ Dor
56405	35180	4	5.445	0.015	−0.04	8830 ± 185	+0.85 ± 0.07	+1.12 ± 0.14	1.56 ± 0.03	other
64491	38723	1	6.221	0.000	0.03	7110 ± 125	+2.37 ± 0.06	+2.06 ± 0.09	0.95 ± 0.03	δ Sct
66920	39041	4	6.320	0.046	+0.02	8200 ± 89	+0.70 ± 0.06	+0.76 ± 0.11	1.62 ± 0.02	const.
68758	40211	4	6.518	0.000	−0.04	8820 ± 132	+0.95 ± 0.08	+0.68 ± 0.15	1.52 ± 0.03	–
73210	42327	4	6.735	0.037	+0.03	7710 ± 84	+0.12 ± 0.24	+0.24 ± 0.24	1.80 ± 0.09	–
73872	1395–2222–1	4	8.317	0.000	+0.03	7790 ± 76		+2.18 ± 0.25	1.03 ± 0.10	δ Sct
74873	43121	1	5.883	0.449	−0.30	10220 ± 471	+1.77 ± 0.05		1.19 ± 0.02	const.
74911	43134	4	8.515	0.000	+0.02	7960 ± 151	+2.18 ± 0.34	+1.61 ± 0.16	1.26 ± 0.06	–
75654	43354	1	6.372	0.000	+0.03	7270 ± 85	+1.98 ± 0.06	+2.11 ± 0.05	1.06 ± 0.02	δ Sct
78316	44798	4	5.236	0.059	−0.98	13500 ± 117	−0.88 ± 0.09		2.25 ± 0.04	other
78661	44984	4	6.474	0.000	+0.03	6830 ± 79	+3.52 ± 0.03	+3.43 ± 0.02	0.53 ± 0.01	other
79025	44979	4	6.473	0.023	+0.03	7830 ± 107	+0.41 ± 0.11	+0.37 ± 0.16	1.74 ± 0.04	const.
79108	45167	4	6.132	0.048	−0.22	9840 ± 259	+1.10 ± 0.08		1.46 ± 0.03	–
79469	45336	4	3.878	0.000	−0.37	10550 ± 346	+1.17 ± 0.12		1.43 ± 0.05	–
80081	45688	4	3.890	0.000	+0.01	8430 ± 219	+0.98 ± 0.06		1.51 ± 0.03	–
81290	46011	2	8.864	0.401	+0.03	7140 ± 645		+1.69 ± 0.11	1.22 ± 0.04	const.
82573	46813	4	5.736	0.000	+0.02	8130 ± 107	+0.42 ± 0.09		1.73 ± 0.04	const.
83041	47018	2	8.789	0.659	+0.03	7630 ± 930	+1.18 ± 0.50	+0.79 ± 0.19	1.58 ± 0.08	δ Sct
83277	47155	2	8.281	0.479	+0.03	7380 ± 690	+1.56 ± 0.27	+1.29 ± 0.10	1.38 ± 0.04	const.
84948	48243	2	8.116	0.000	+0.02	6780 ± 64	+1.62 ± 0.41	+0.89 ± 0.19	1.55 ± 0.08	δ Sct
87271	49328	1	7.139	0.785	−0.40	10680 ± 254	+0.29 ± 0.28	+0.66 ± 0.07	1.64 ± 0.03	δ Sct
87696	49593	4	4.479	0.017	+0.02	7950 ± 76	+2.21 ± 0.01	–	1.02 ± 0.00	δ Sct

Table A1 – *continued*

HD	HIP/TYC	mem.	m_V (mag)	A_V (mag)	B.C. (mag)	T_{eff} (K)	$M_{V,\,Hip}$ (mag)	$M_{V,\,Gaia}$ (mag)	$\log L/L_\odot$	var?
89239	50459	4	6.525	0.036	−0.36	10500 ± 235	+0.71 ± 0.13	–	1.62 ± 0.05	–
91130	51556	1	5.902	0.000	+0.02	8130 ± 152	+1.44 ± 0.05	–	1.32 ± 0.02	const.
97411	54742	4	6.098	0.076	−0.30	10250 ± 208	+0.09 ± 0.24	–	1.87 ± 0.09	–
97773	54981	3	7.552	0.021	+0.03	7420 ± 104	+0.91 ± 0.34	–	1.54 ± 0.14	–
97937	55033	3	6.649	0.000	+0.03	7190 ± 76	+2.53 ± 0.08	+2.32 ± 0.06	0.97 ± 0.02	–
98353	55266	4	4.755	0.000	+0.01	8410 ± 184	+0.91 ± 0.04	–	1.54 ± 0.02	other
98772	55564	4	6.021	0.000	+0.01	8330 ± 156	+1.33 ± 0.06	–	1.37 ± 0.03	–
100546	56379	3	6.696	0.197	−0.40	10720 ± 193	+1.57 ± 0.09	+1.31 ± 0.08	1.38 ± 0.03	other
100740	56553	4	6.563	0.000	+0.02	7900 ± 132	+1.42 ± 0.09	+1.34 ± 0.14	1.33 ± 0.04	–
101108	56768	2	8.847	0.023	+0.03	7800 ± 75	–	+1.32 ± 0.22	1.37 ± 0.09	const.
102541	57567	2	7.946	0.088	+0.03	7690 ± 108	+2.50 ± 0.17	+2.62 ± 0.08	0.85 ± 0.03	δ Sct
105058	58992	1	8.873	0.026	+0.03	7670 ± 113	+2.41 ± 0.38	+1.00 ± 0.27	1.50 ± 0.11	δ Sct
105199	2527–707–1	4	9.815	0.000	+0.03	7750 ± 117	–	+2.47 ± 0.41	0.91 ± 0.17	–
105260	59107	3	9.180	0.000	+0.03	7260 ± 89	–	+2.28 ± 0.13	0.99 ± 0.05	–
106223	59594	1	7.416	0.313	+0.03	7000 ± 783	+1.65 ± 0.17	+1.37 ± 0.09	1.35 ± 0.04	const.
107223	60137	4	8.187	0.359	−0.15	9490 ± 575	–	+0.65 ± 0.18	1.64 ± 0.07	const.
107233	60134	1	7.361	0.000	+0.03	7220 ± 76	+2.62 ± 0.12	+2.87 ± 0.05	0.75 ± 0.02	–
108283	60697	4	4.910	0.155	+0.03	7140 ± 50	+0.12 ± 0.04	–	1.85 ± 0.02	–
108714	60933	4	7.718	0.000	+0.01	8310 ± 329	+1.40 ± 0.23	+1.34 ± 0.31	1.34 ± 0.09	–
108765	60957	4	5.671	0.097	−0.02	8720 ± 227	+0.95 ± 0.05	–	1.52 ± 0.02	–
109738	9228–358–1	1	8.284	0.086	+0.03	7600 ± 102	–	+2.17 ± 0.10	1.03 ± 0.04	δ Sct
109980	61692	4	6.346	0.000	+0.03	7670 ± 120	+2.19 ± 0.06	–	1.02 ± 0.03	other
110377	61937	4	6.212	0.000	+0.03	7700 ± 80	+2.22 ± 0.04	+1.94 ± 0.05	1.01 ± 0.02	δ Sct
110411	61960	1	4.864	0.063	−0.06	8970 ± 112	+2.00 ± 0.02	–	1.10 ± 0.01	const.
111005	62318	2	7.962	0.077	+0.02	6790 ± 65	+1.86 ± 0.26	+1.98 ± 0.15	1.11 ± 0.06	const.
111164	62394	4	6.096	0.000	+0.02	8210 ± 77	+1.49 ± 0.07	+1.92 ± 0.13	1.30 ± 0.03	–
111604	62641	1	5.875	0.000	+0.03	7640 ± 105	+0.67 ± 0.08	+0.68 ± 0.10	1.63 ± 0.03	δ Sct
111786	62788	1	6.136	0.017	+0.03	7490 ± 100	+1.99 ± 0.05	+2.11 ± 0.07	1.10 ± 0.02	δ Sct
111893	62825	4	6.290	0.000	+0.03	7710 ± 92	+1.07 ± 0.10	–	1.47 ± 0.04	–
112097	62933	4	6.237	0.000	+0.03	7330 ± 95	+2.31 ± 0.11	–	0.97 ± 0.04	δ Sct
113848	63948	4	6.014	0.000	+0.01	6620 ± 49	+2.53 ± 0.08	–	0.89 ± 0.03	–
114879	64477	4	8.920	0.000	+0.02	7960 ± 81	–	+1.80 ± 0.24	1.18 ± 0.10	–
114930	64525	4	9.017	0.000	+0.03	7080 ± 73	+3.35 ± 0.33	+2.36 ± 0.14	0.96 ± 0.06	–
118623	66458	4	4.901	0.000	+0.03	7400 ± 91	+0.98 ± 0.07	+1.22 ± 0.12	1.51 ± 0.03	–
119288	66860	4	6.162	0.000	+0.01	6560 ± 57	+3.35 ± 0.03	–	0.56 ± 0.01	other
120500	67481	1	6.597	0.040	+0.02	8250 ± 65	+0.62 ± 0.18	+0.88 ± 0.19	1.65 ± 0.07	δ Sct
120896	67705	1	8.501	0.000	+0.03	7370 ± 100	±	+1.56 ± 0.16	1.27 ± 0.06	δ Sct
123299	68756	4	3.644	0.003	−0.21	9790 ± 362	−1.20 ± 0.03	–	2.38 ± 0.01	other
125162	69732	1	4.176	0.101	−0.04	8840 ± 196	+1.66 ± 0.01	–	1.23 ± 0.00	δ Sct
125489	70022	4	6.178	0.033	+0.02	7970 ± 76	+2.14 ± 0.05	–	1.04 ± 0.02	–
125889	7294–813–1	2	9.835	0.126	+0.03	7320 ± 100	–	+2.24 ± 0.28	1.00 ± 0.11	const.
128167	71284	4	4.467	0.000	+0.02	6720 ± 45	+3.47 ± 0.01	–	0.51 ± 0.00	–
130158	72323	4	5.609	0.092	−0.46	10960 ± 322	−1.27 ± 0.17	−0.43 ± 0.31	2.41 ± 0.07	other
130767	72505	1	6.903	0.000	−0.09	9170 ± 234	+1.41 ± 0.16	+1.36 ± 0.09	1.36 ± 0.04	const.
138527	76069	2	6.217	0.140	−0.48	11080 ± 200	+0.29 ± 0.14	–	1.79 ± 0.05	–
141569	77542	1	7.123	0.411	−0.27	10080 ± 291	+1.39 ± 0.15	+1.48 ± 0.10	1.31 ± 0.04	–
141851	77660	4	5.090	0.000	+0.02	8100 ± 125	+1.61 ± 0.04	–	1.26 ± 0.01	const.
142703	78078	1	6.113	0.000	+0.03	7200 ± 89	+2.57 ± 0.04	–	0.87 ± 0.02	δ Sct
142994	6791–1423–1	1	7.173	0.023	+0.03	6960 ± 76	–	+1.22 ± 0.12	1.41 ± 0.05	δ Sct
143148	7329–1376–1	4	7.388	0.012	+0.03	7180 ± 85	–	+1.96 ± 0.08	1.12 ± 0.03	const.
144708	79005	4	5.756	0.201	−0.35	10460 ± 397	+0.30 ± 0.15	–	1.78 ± 0.06	–
145782	79689	4	5.617	0.106	+0.02	8230 ± 85	−0.05 ± 0.08	–	1.92 ± 0.03	const.
149130	81329	2	8.475	0.286	+0.03	6950 ± 173	+1.44 ± 0.53	+1.45 ± 0.13	1.32 ± 0.05	const.
149303	80953	3	5.658	0.000	+0.02	8170 ± 221	+1.45 ± 0.09	–	1.32 ± 0.04	const.
153747	83410	1	7.403	0.115	+0.02	8190 ± 78	+1.01 ± 0.25	+0.88 ± 0.11	1.55 ± 0.04	δ Sct
153808	83207	4	3.901	0.102	−0.34	10440 ± 165	+0.41 ± 0.01	–	1.73 ± 0.01	–
154153	83650	2	6.184	0.335	+0.03	7400 ± 567	+1.63 ± 0.09	–	1.25 ± 0.04	const.
156954	84895	3	7.670	0.000	+0.03	7070 ± 61	+2.90 ± 0.16	+2.90 ± 0.07	0.74 ± 0.03	const.
159082	85826	4	6.416	0.184	−0.47	11020 ± 199	+0.58 ± 0.12	+0.62 ± 0.18	1.67 ± 0.05	–
160928	86847	4	5.872	0.000	+0.02	7870 ± 91	+1.58 ± 0.06	–	1.27 ± 0.02	–
161223	427–1650–1	1	7.443	0.404	+0.03	7430 ± 107	–	+0.32 ± 0.16	1.77 ± 0.06	δ Sct
161868	87108	4	3.740	0.052	−0.10	9210 ± 151	+1.20 ± 0.01	–	1.42 ± 0.01	–
168740	90304	1	6.122	0.020	+0.03	7670 ± 121	+1.84 ± 0.05	+1.87 ± 0.08	1.16 ± 0.02	δ Sct

Table A1 – *continued*

HD	HIP/TYC	mem.	m_V (mag)	A_V (mag)	B.C. (mag)	T_{eff} (K)	$M_{V,\,Hip}$ (mag)	$M_{V,\,Gaia}$ (mag)	$\log L/L_\odot$	var?
168947	7913–1173–1	1	8.114	0.124	+0.03	7510 ± 101	–	+1.10 ± 0.18	1.46 ± 0.07	δ Sct
169009	90083	4	6.322	0.665	−0.27	10120 ± 441	+0.60 ± 0.30	+1.46 ± 0.11	1.32 ± 0.04	–
169022	90185	4	1.802	0.112	−0.18	9640 ± 125	−1.52 ± 0.02	–	2.51 ± 0.01	–
169142	6856–876–1	3	8.152	0.000	+0.02	6700 ± 322	–	+2.81 ± 0.07	0.78 ± 0.03	–
170000	89908	4	4.223	0.009	−0.77	12430 ± 139	−0.62 ± 0.08	–	2.15 ± 0.03	other
170680	90806	1	5.120	0.107	−0.22	9860 ± 302	+0.84 ± 0.04	–	1.56 ± 0.02	–
172167	91262	2	0.074	0.042	−0.13	9400 ± 384	+0.61 ± 0.01	–	1.66 ± 0.00	δ Sct
174005	92296	1	6.493	0.230	+0.03	7790 ± 138	−0.56 ± 0.27	+0.15 ± 0.12	1.84 ± 0.05	–
175445	92884	4	7.781	0.129	−0.07	9060 ± 333	+1.50 ± 0.25	–	1.30 ± 0.10	–
177756	93805	4	3.427	0.000	−0.57	11460 ± 158	+0.53 ± 0.05	–	1.69 ± 0.02	–
179791	94478	4	6.472	0.000	+0.02	8090 ± 118	+0.62 ± 0.27	+0.20 ± 0.22	1.82 ± 0.09	const.
181470	94932	4	6.243	0.062	−0.26	10050 ± 186	−0.22 ± 0.13	+0.37 ± 0.27	1.99 ± 0.05	–
183007	95823	3	5.702	0.000	+0.03	7670 ± 106	+1.52 ± 0.05	–	1.21 ± 0.02	–
183324	95793	1	5.783	0.330	−0.22	9840 ± 150	+1.52 ± 0.05	–	1.29 ± 0.02	δ Sct
184190	7936–1366–1	4	9.737	0.138	+0.03	7160 ± 95	–	+2.71 ± 0.15	0.82 ± 0.06	–
184779	7944–1500–1	1	8.911	0.000	+0.03	7130 ± 81	–	+2.06 ± 0.14	1.08 ± 0.06	const.
187949	97849	4	6.481	0.000	+0.02	7970 ± 99	+1.10 ± 0.15	–	1.46 ± 0.06	other
188164	98346	1	6.373	0.077	+0.02	8160 ± 64	+1.18 ± 0.11	+1.28 ± 0.15	1.39 ± 0.06	const.
188728	98103	4	5.285	0.047	−0.21	9810 ± 155	+1.10 ± 0.04	–	1.46 ± 0.01	–
191850	8392–2637–1	1	9.682	0.022	+0.03	7370 ± 95	–	+1.75 ± 0.29	1.20 ± 0.12	δ Sct
192640	99770	1	4.946	0.043	+0.02	7960 ± 92	+1.75 ± 0.02	–	1.20 ± 0.01	δ Sct
193281	100288	3	6.629	0.100	+0.02	8020 ± 72	–	+0.51 ± 0.18	1.70 ± 0.07	const.
196821	101919	4	6.074	0.000	−0.30	10250 ± 58	−0.64 ± 0.19	–	2.16 ± 0.07	–
198160	102962	1	6.173	0.018	+0.02	7930 ± 77	+1.74 ± 0.11	–	1.20 ± 0.04	–
198161	102962	1	6.518	0.018	+0.02	7900 ± 77	+2.09 ± 0.11	–	1.07 ± 0.04	–
200841	104042	4	8.270	0.362	−0.26	10070 ± 319	–	+0.18 ± 0.24	1.83 ± 0.10	–
201019	104408	3	8.380	0.167	+0.02	6660 ± 257	+2.27 ± 0.31	+1.63 ± 0.15	1.25 ± 0.06	–
201184	104365	4	5.307	0.072	−0.25	9990 ± 189	+1.53 ± 0.04	–	1.29 ± 0.01	–
204041	105819	1	6.454	0.034	+0.02	8090 ± 74	+2.07 ± 0.10	+2.10 ± 0.05	1.06 ± 0.02	const.
204754	106052	4	6.135	0.666	−0.80	12550 ± 108	−2.49 ± 0.25	−1.86 ± 0.31	2.90 ± 0.10	–
204965	106171	4	6.011	0.060	+0.01	8420 ± 131	−0.05 ± 0.09	+0.15 ± 0.13	1.92 ± 0.04	–
207978	107975	4	5.524	0.053	−0.01	6330 ± 99	+3.28 ± 0.02	–	0.59 ± 0.01	–
210111	109306	1	6.375	0.000	+0.03	7470 ± 103	+1.91 ± 0.09	+1.92 ± 0.04	1.13 ± 0.02	δ Sct
210418	109427	4	3.520	0.084	−0.03	8730 ± 226	+1.18 ± 0.05	–	1.43 ± 0.02	–
212061	110395	4	3.844	0.006	−0.30	10250 ± 256	+0.33 ± 0.11	–	1.77 ± 0.05	–
212150	110116	4	6.612	0.215	−0.24	9940 ± 377	−0.60 ± 0.27	−0.21 ± 0.19	1.98 ± 0.08	–
213669	111411	2	7.409	0.000	+0.03	7350 ± 124	+2.24 ± 0.16	+2.10 ± 0.09	1.06 ± 0.04	δ Sct
214454	111674	4	4.644	0.000	+0.03	7380 ± 113	+1.04 ± 0.02	–	1.48 ± 0.01	–
216847	113351	2	7.059	0.006	+0.03	7340 ± 97	+1.16 ± 0.16	+1.20 ± 0.13	1.42 ± 0.05	const.
217782	113788	4	5.085	0.281	−0.08	9140 ± 144	−0.75 ± 0.14	–	2.20 ± 0.06	other
218396	114189	1	5.953	0.000	+0.03	7230 ± 95	+2.98 ± 0.06	+2.92 ± 0.06	0.73 ± 0.02	γ Dor
220061	115250	3	4.581	0.000	+0.03	7700 ± 87	+1.10 ± 0.04	–	1.46 ± 0.02	δ Sct
220278	115404	3	5.441	0.000	+0.03	7610 ± 101	+1.36 ± 0.11	–	1.35 ± 0.04	–
221756	116354	1	5.557	0.093	−0.01	8630 ± 200	+0.94 ± 0.05	–	1.52 ± 0.02	δ Sct
222303	4292–245–1	3	9.159	1.001	+0.03	6960 ± 69	–	+0.17 ± 0.21	1.83 ± 0.09	–
223352	117452	2	4.572	0.062	−0.23	9930 ± 197	+1.39 ± 0.02	–	1.35 ± 0.01	–
228509	3151–1876–1	3	9.237	0.105	+0.03	7220 ± 50	–	+0.68 ± 0.36	1.63 ± 0.14	–
290799	4767–765–1	1	10.703	0.022	+0.02	7940 ± 71	–	+3.10 ± 0.25	0.66 ± 0.10	δ Sct
294253	4770–1225–1	1	9.645	0.228	−0.37	10580 ± 211	–	+1.49 ± 0.28	1.30 ± 0.11	const.

This paper has been typeset from a TEX/LATEX file prepared by the author.